This article has been published in the Journal of Raman Spectroscopy, 2017 Vol. 48, 384–392.

Title: *Ex vivo* detection and characterization of remineralized carious dentin, by nanoindentation and single point Raman spectroscopy, after amalgam restoration.

Short title: Remineralization of carious dentin after restoration.

Authors: Manuel Toledano[1*], Estrella Osorio[1], Fátima S. Aguilera[1], Inmaculada Cabello[1], Manuel Toledano-Osorio[1], Raquel Osorio[1].

Institution: [1]University of Granada, Faculty of Dentistry, Dental Materials Section.

Address: [1] University of Granada, Faculty of Dentistry, Dental Materials Section
Colegio Máximo de Cartuja s/n
18071 – Granada - Spain.

*Corresponding author: Prof. Manuel Toledano
University of Granada, Faculty of Dentistry
Dental Materials Section
Colegio Máximo de Cartuja s/n
18071 – Granada - Spain.
Tel.: +34-958243788
Fax: +34-958240809
Email: toledano@ugr.es

Abstract

The aim of this study was to assess the mechanical and chemical performance of sound and caries-affected dentin (CAD), after Zn-free *vs* containing amalgam restorations placement and thermocycling. Dentin surfaces were studied by Atomic Force Microscopy (AFM) analysis for surface morphological characterization (including fibril diameter assessment), nano-indentation (to measure nano-hardness-Hi and modulus of Young-Ei), and single point Raman spectroscopy for chemical analysis. Measurements were performed before amalgam placement, after amalgam removal, and after 3 months of thermocycling (100,000cy/5 ºC and 55 ºC). Restorations increased both Hi and Ei at intertubular dentin of CAD. The highest values of Hi were achieved at intertubular dentin after restoring with Zn-containing amalgams. Remineralization of dentin was attributed to the increase of both amorphous and crystalline new mineral, as lower degrees of crystal imperfections in junction with crystal disorders, and improvement in structural stability of collagen were found. Higher presence of minerals were also confirmed after the decrease of fluoridated apatite and the increase of the total water content. Proteoglycans, lipids, and proteins, augmented in both sound and CAD, providing support for the mineral growing. The increase of bands assigned to vibration of carbonate calcium phosphate contributed to a decrease of crystallinity.

Key words: Dentin, remineralization, Raman, amalgam.

Introduction

The dentin itself is a mineralized tissue composed of 50% by volume of crystals of carbonated calcium hydroxyapatite [$Ca_{10}(PO_4)_6(OH)_2$], where PO_4^{3-} or OH^- can be substituted by CO_3^{2-}[1]. The organic matter represents 18% by volume, which is largely a felt-work of type I collagen (90%) and noncollagenous proteins (10%) such as glycosaminoglycans, phosphorilated proteins and proteoglycans[2]. Proteoglycans, which play an important role in the mechanical and structural integrity of the tissue[3], have been proposed to act as bridges between continuous collagen fibrils, thus indirectly facilitating the deposition of the extrafibrillar apatite in mineralized tissues. Approximately, 10 vol% of the dentin content is fluid. The mineral in dentin is located either in the gaps between collagen molecules (intrafibrillar) or attached to the collagen fibrils (extrafibrillar)[4]. Type I collagen molecules are composed of three supercoiled polypeptide chains of about 290 nm in length, held together by water bridges and hydrophobic cross-links. Five tropocollagen molecules stagger longitudinally, overlapping by about one quarter of their length, to form a microfibril about 4 nm in diameter. The microfibrils aggregate with their long axes in parallel to form collagen fibrils[4]. This applies in the case of sound dentin, but not when dentin is damaged by the carious process.

Dental caries is a common oral disease that many people have experienced at some point in their live. It is an irreversible microbial disease that affects the calcified structures of the tooth. Carious dentin arises from the destruction of this structure by acid-forming bacteria found in dental plaque[5]. Clinically, dental caries is characterized by progressive demineralization of inorganic structures, and destruction of organic structures if dentin results infected. Caries-affected dentin is partially demineralized and more porous than non-carious dentin with a predominantly intact collagen matrix, whose collagen fibrils retain their banded structure and intermolecular crosslinks[6]. It should be preserved during clinical treatment because it is remineralizable and serves as a suitable substrate for tooth repair[7] and physiologic or therapeutic remineralization[8].

By the time being, amalgam continues to play a major role in restorative dentistry, today[9], though it is not an ideal material, as the cosmetic appearance is poor and cannot bond to tooth[10]. Amalgam is being discontinued in response to global concerns about mercury in the environment, but the evidence brought by studies assessing the environmental risks is based on estimations and assumptions; therefore, no concrete conclusions can be drawn[11].The Food and Drug Administration (FDA) and the American Dental Association (ADA) support amalgam as safe and effective material for dental restorations[12,13]. The FDA also claims that the levels of exposure to the mercury from amalgams are well below levels actually known to cause adverse effects, and notes that amalgam is a commonly used device with a low frequency of adverse events reported to the agency[14]. With a failure rate nearly double that of amalgam[15], the increasing trend to replace amalgam with resin composite could be detrimental for patients. Removal of these restorations leads to loss of sound tooth structure with concomitant weakening of the tooth and possible pulpal injury[16], translating to the need for more complex restorations and, eventually, total tooth loss[17]. It has been demonstrated that Sn, Ca, P and Zn diffuse the outer demineralized layer and accumulate *in situ* over time forming poorly soluble deposits of oxides and hydroxides[18], generating corrosion-sealing products at the interface. These elements protect the dentin interface against microleakage and recurrent decay, as oral fluids, bacterial enzymes and bacteria cannot penetrate through this natural sealing barrier[17]. Most of the times, it is not necessary to line the base of the cavity prior to condensating

the amalgam, and in large cavities, dentin pins may be required as an alternative form of retention[19]. Additionally, Zn-containing amalgams submitted to mechanical stimuli have contributed to create new crystalline mineral deposits on the partially mineral-depleted subjacent substrate of the caries-affected dentin[14]. Furthermore, after thermocycling, new mineral aggregated on the carious dentin below the amalgams restoration[20], but to know if they are crystalline or amorphous in order to infer their clinical performance, must be ascertained.

The mechanical behavior of both peritubular and intertubular dentin is an important aspect contributing to the outstanding durability of teeth, and thus an improved understanding of such heterogeneous character is desired[2]. Elastic materials strain instantaneously when load is removed[21]. The elastic response between the peritubular and intertubular dentin regions has long been compared and it has been established that peritubular dentin is a highly mineralized material harder and more elastic than the more compliant intertubular dentin[22]. This conjecture is applicable to the untreated sound dentin, but to ascertain this performance after amalgam restoration treatment in both sound and caries-affected dentin must be determined. Scanning probe microscopes and, in particular, the atomic force microscope have facilitated the imaging and analysis of biological surfaces with little or no sample preparations[4].

Raman spectroscopy is an analytical technique able to measure the molecular composition by providing a spectrum that contains information regarding all the chemical bonds present within the sample[23] for investigating molecular species. Micro-Raman mapping technique has been a powerful method to directly analyze the dentin interface and the mineral content, and distribution, after placing the restorative and the application of mechanical[14] and thermal stimuli. Single point Raman spectra, permits to image a line profile thorough a series of point-to-point sampling. Hence, the total acquisition time equals the number of sample position observed, plus any overhead associated with sample motion. At first glance, line imaging appears quite similar, with an end result of a data set consisting of intensity *vs* Raman shift and position along a line[24]. It furnishes biochemical specificity because it is based on spectral peaks specific to the biochemical and structural properties of hard tissues mineralization[5,25,26].This technique is sufficiently sensitive to differences in mineral and organic compositions that can be used to identify damaged, damage-susceptible or restored areas, and possibly explain why certain regions of dentin are subject to decay. By identifying and imaging the Raman spectral features characteristics of carious regions, the structural differences associated with carious dentin[27] and further remineralization can be assessed. Combining the two technologies takes advantage of their synergies for characterizing lesions and for providing objective nanomechanical and biochemical information.

The null hypothesis is that there are no differences in dentin mineralization, expressed in term of mechanical and chemical properties, of sound and caries-affected substrata after removal of Zn-free *vs* Zn-containing amalgam restorations.

Materials and Methods

Specimens preparation and thermocycling

Nine extracted carious third molars without opposing occlusion were employed for the study. They were stored in 0.01% (w/v) thymol at 4º C for less than 1 month. Teeth were collected after written patients' informed consent (20 to 40 years of age), under a protocol approved by the Institution Review Board (891/2014). The inclusion criteria for carious dentin substrate were that the caries lesion, surrounded by sound dentin, was limited to the occlusal surface and it was extended at least half the distance from the enamel-dentin junction to the pulp chamber. To obtain caries affected dentin, grinding

was performed by using the combined criteria of visual examination, surface hardness using a dental explorer, and staining by a caries detector solution (CDS, Kuraray Co., Ltd., Osaka, Japan). Using this procedure it was removed all soft stainable, carious dentin. It was left the relatively hard, caries-affected dentin, non stainable, on the experimental side. Flat mid-coronal sound dentin, and caries affected dentin surfaces surrounded by normal dentin, were exposed using a hard tissue microtome (Accutom-50; Struers, Copenhagem, Denmark) equipped with a slow-speed, water-cooled diamond wafering saw (330-CA RS-70300, Struers, Copenhagen, Denmark). Molars were transversally sectioned (Isomet 4000, Buehler, Lake Bluff, IL, USA) at the mid-coronal portion of each tooth, bucco-lingually, to produce dentin discs (2.5 mm thick), and were polished[28,29] through SiC abrasive papers up to 4,000-grit with a final polishing procedure performed with diamond pastes (Buehler-MetaDi, Buehler Ltd.), through 1 μm down to 0.25 μm. The specimens were treated in ultrasonic bath (Model QS3, Ultrawave Ltd, Cardiff, UK) containing deionized water [pH 7.4] for 5 min at each polishing step.

Teeth were divided into three groups (n=3), and two third of teeth were restored with amalgam (with or without zinc) and one third remained untreated. Two self threading titanium retentive pins (4.4 mm length) (STP Restorative Dentsply Maillefer, Ballaigues, Switzerland) were used to retain the amalgam restorations[18], by using copper bands (Copper Bands, Hard. AB Dentatus, Spånga, Sweden), surrounding the prepared dentin discs. A tile of Zn-free *vs*. Zn-containing dental amalgam was condensed on top of the disc surfaces in a layer of at least 3 mm thick (Graphic 1). The detailed composition of each amalgam is shown in Table 1. Finally, the amalgam surfaces were finished with hand instruments. The other third remained untreated as control.

Teeth were stored for 24 hours in simulated body fluid solution (SBFS), pH 7.45, at 37 ºC, and then submitted to the test of thermal cycling (100,000 cycles, ranging from 5 ºC to 55 ºC every 30 seconds, during 3 months) (SD Mechatronik GmbH, Germany), in BSFS. The amalgam tiles were removed from the discs by cutting away the amalgam around the retentive pins. All specimens were then submitted to Atomic Force Microscopy (AFM) analysis to undertake the nanoindentation's test and for fibril diameter assessment; Raman analysis of the dentin surfaces were also accomplished. To facilitate the identification of caries-affected dentin areas, they were marked with a diamond point, and localized trough a XY 330 lines/mm grating scale, where the different rows and columns of grating are equally spaced through the whole area of the specimen.

Atomic Force Microscopy (AFM) analysis

Nano-indentation test

An atomic force microscope (AFM Nanoscope V, Digital Instruments, Veeco Metrology group, Santa Barbara, CA, USA) equipped with a Triboscope indentor system (Hysitron Inc., Minneapolis, MN) was employed in this study. The process was undertaken inside a wet cell in a fully hydrated state (Digital Instrument, Santa Barbara, CA, USA). The nanoindentation process was performed using a Berkovich diamond indenter with a tip radius of 20 nm. Ten indentations with a peak load of 4000 nN and a time function of 10 s were performed on each dentin disc. From these experiments we obtained the nanohardness (Hi) and the nanoindentation modulus (E_i) of the samples. At this point, we would like to mention that the nanoindentation modulus obtained by this method is usually referred to as Young's modulus in the literature, which however should not be confounded with the Young's modulus obtained at the macroscopic level

by traction/compression experiments. Nevertheless, we keep Young's modulus terminology for the nanoindentation modulus along this manuscript, as it is the usual case in most of the literature.

In nanoindentation experiments the indenter was progressively (at a constant rate) pressed over the sample up to a peak load of 4000 μN (loading part of the experiment) and, afterwards, the load was progressively released to zero value (unloading part of the experiment). From these experiments the load, *F*, was obtained as a function of the penetration depth, *h*, of the indenter in the sample. From the slope of these load-vs.-depth curves, the nanoindentation modulus (Young's modulus) can be obtained by application of different theoretical models[30,31]. One of these is the Oliver-Pharr method, which is based on a continuum, isotropic, homogeneous elastic contact model to determine the reduced modulus, E_r. In this model the slope, S, of the unloading portion of the load-vs. depth data is used to obtain E_r according to the following equation[31]:

$$S = \frac{dF}{dh} = \frac{2}{\sqrt{\pi}} E_r \sqrt{A}\,, \qquad (1)$$

where A is the projected contact area of the hardness impression of the indenter. Then, E_i of the sample is obtained through the following expression:

$$\frac{1}{E_r} = \frac{\left(1-\nu_{ind}^2\right)}{E_{ind}} + \frac{\left(1-\nu_i^2\right)}{E_i}, \qquad (2)$$

In this expression "*i*" subscript refers to the tested sample and "*ind*" subscript to the indenter. ν and E are the Poisson's ratio and the Young's modulus, respectively. For hard materials, as dentin, Usually, $E_{ind} >> E_i$ and, thus, the contribution of the indenter in equation (2) can be neglected. With regard to the nanohardness of the sample, H, it is defined as:

$$H = \frac{F_{max}}{A}\,, \qquad (3)$$

where F_{max} is the peak load. In this work, values of nanohardness and Young's modulus were automatically calculated by using the software of the AFM (Triboscan Quasi version 8.4.2.0 Hysitron, Inc).

Fibril diameter assessment

The disks surfaces were scanned using a tapping mode /atomic force microscopy (TM /AFM) (Nanoscope V, Digital Instruments, Veeco Metrology Group, Santa Barbara, CA, USA). The tapping mode was performed using a 1–10 Ohm-Cm phosphorus (n) doped Si tip. Changes in vertical position provide the height of the images, registered as bright and dark regions. The tip sample was maintained stable through constant oscillation amplitude. A data scale of 1,504 μm and a slow scan rate (0.1 Hz) were employed. Five phase images and five three-dimensional (3D) digital images (2x2 μm) were captured for each specimen.

Assembled in a single user interface, NanoScope Analysis. Ink software served as a semi-automatic analysis tool capable of measuring several geometrical properties (length, volume and angles). NanoScope Analysis can open image data files from NanoScope (v5.30v2). The selected image is loaded in the main panel so individual complexes can be measured. Each complex can be labelled with a specific alphanumeric identifier, and it will appear in the adjacent window for volume and length analysis. Fibrils width can be estimated by measuring directly one part of the fibril with the line

tool.

Collagen fibril diameter was determined from the 2x2 μm images by section analysis using data that had been modified only by plane fitting. Five fibrils were analyzed from each image. Measurements were corrected for tip broadening[30] by the equation $e=2r$, where e is the error in the horizontal dimension and r is the tip's radius[31].

As the normality assumption of the data was valid, numerical data were analysed by two-way ANOVA and Student-Newman-Keuls multiple comparisons ($P<0.05$). Analysis of interactions was included. Differences between attained values at pre and post-amalgam conditions were analyzed by Student's t test ($P<0.01$).

Single point Raman spectra analysis

A dispersive Raman spectrometer/microscope (Horiba Scientific Xplora, Villeneuve d´Ascq, France) was used to analyze dentin surfaces. A near-infrared diode laser spot size of ≈ 0.5μm^2 operate dat 785 nm was used to induce the Raman scattering effect (100 mW sample power) and an X100/0.90 NA air objective were employed. The spectrometer was equipped with a liquid-nitrogen-cooled CCD detector (DR-324B-FI-327, And or Technology LTD, UK). Raman signal was acquired using a 600-lines/mm grating centered between 400 and 3,500 cm^{-1}.Calibration of the wavelength and intensity was performed according to manufacturer's specification using a silicon standard and calibration system integrated with the LabSpec 6.3 Analysis software. In order to ascertain that measured intensities are meaningful, all measurements were performed under the same laser excitation power and the same measurements conditions. Moreover, a reference material was measured daily to evaluate any changes in the system performance. The signal corresponding to this reference material was stable (± 5). For microspectroscopy, the confocal hole size was set at 300μm and the slit size at 100 μm. The spectral resolution of the system was 6.25cm^{-1}. A total of 50 spectra were used in the analysis for each specimen. Raman spectra were taken over each specimen surface area in a lineal sequence of 25 μm, with 2.5 μm point interval. Spectra were measured using 10 s acquisition time with 5 accumulations; imaging was performed with a X100 objective.

At this point, the Raman spectroscopic peaks of both mineral and organic components found in sound and caries-affected dentin were assessed.

Mineral components:

1. Bands assigned to vibrations of carbonated calcium phosphate in an apatitic lattice are 430 and 451 cm^{-1} (v_2 mode)[27].
2. Symmetric bending mode (v_2) PO_4^{3-}, at 431 and 446 cm^{-1} peaks. These two bands are present in sound and carious substrata. In caries spectra, 431 cm^{-1} peak intensity is greater than 446 cm^{-1} peak[5].
3. Changes in fluoridated apatite (575 cm^{-1}) reflect bacterial metabolic activity and organic content[32].
4. Peaks at 579, 590, 608, 614 cm^{-1} (v_4 asymmetric bending mode PO_4^{3-}). Band pair 579, 590 shows greater intensity in the caries spectrum but weaker intensity in the sound spectrum[5].
5. V_1 toward 950 cm^{-1} indicates amorphous calcium phosphate in an apatitic lattice[5].
6. Peak at 954 cm^{-1}, representative of PO_4^{3-} v_1 symmetric vibration, is a marker for calcification of the ECM[23].
7. Asymmetric peak at 956 cm^{-1}indicates additional substituted or amorphous-like apatite species[27].

8. The symmetric stretching vibration (v_1 mode) of phosphate PO_4^{3-}, at 959 cm^{-1} dominates both sound and carious dentin[5].
9. 960 $cm^{-1}$is linked with nonaromatic mode $v_1PO_4^{3-}$[33].
10. Stoichiometric HAP is found in phosphate v_1 vibration, found at 963 cm^{-1}[27].
11. Strong monohydrogen phosphate v_1 vibration (~1003 cm^{-1}) indicates areas where active remodeling are occurring, performing as a good probe of mineral structure and substitution, in junction with the phosphate v_1 vibration (~960 cm^{-1})[27].
12. Peaks at 1023, 1043, 1052 (asymmetric stretching $v_3$modeof phosphate PO_4^{3-}), and 1069 (symmetric stretching mode of type B CO_3^{2-})cm^{-1}, increase in the caries spectrum[5]. 1069 cm^{-1} peak assigned to both PO_4^{3-} and type-B CO_3^{2-} do not change between sound and carious dentin, despite the loss of carbonate with demineralization[5]. Strong intensity peak at 1072 cm^{-1} indicates as substantial amount of B-type carbonate substitution in this phosphate mineral[27].
13. Peak at 1104 cm^{-1} represent the symmetric stretching mode of type-A CO_3^{2-}[32].
14. The intensity ratio plot shows enhanced 431/ 959, 446/ 959, 579/ 959, 590/ 959, 1043/ 959, 1069/ 959 at the carious lesion[5].
15. The crystallinity of biological apatites can be estimated by the value of the 1020/1030 ratio intensity (1020 cm^{-1}, nonstoichiometric apatites containing HPO_4^{2-}, CO_3^{2-}, and vacancies; 1030 cm^{-1}, stoichiometric apatites) and the increase at 1145 cm^{-1} peak[34].

Organic components:

1. Peaks at 855 and 871 cm^{-1} indicates C-C stretch of proline and hydroxyproline[27].
2. Bands assigned to vibrations at 920 cm^{-1} are linked with P-OH stretching and the ν(C-C) of hydroxylated proline[33].
3. Collagen (proline/hydroxyproline/C-C skeletal of collagen backbone), is indicated by bands at 937 cm^{-1}[23].
4. Phenylalanine (C-C aromatic ring) is represented by peaks at 1001cm^{-1}[23].
5. Proteoglycans are found at 1062 cm^{-1}[23].
6. Lipids and proteins (CH_2 and amide I) are identified with peaks at 1448 and 1656 cm^{-1}[23].
7. Peaks at 1610-1620 $cm^{-1}$are assigned to tyrosine side chain vibration[32].
8. Peaks at 1637 cm^{-1} are assigned to amide I ($C_1O_1…H_2O$)[32].
9. Peaks at 1662$cm^{-1}$are assigned to amide I ($C_2O_2…H_4N_4$)[32].
10. Peaks at 1694$cm^{-1}$are assigned to amide I ($C3O_3…H_2O$)[32].
11. Peaks at 3350-3400 cm^{-1} are indicative of amide B[32].
12. Peaks at 3070-3085 cm^{-1} are indicative of amide A[32].
13. The organic to inorganic ratio of dentin components was assessed from the band peaks of the organic amide I (1674 cm^{-1}) with the peaks of the inorganic phosphatic component at 959 cm^{-1}[35].
14. The decrease of the 3420 cm^{-1} shoulder indicates total water content decreases[34].

Results and Discussion

Results confirm that Zn-containing amalgam restorations remineralized the partially mineral-depleted in caries-affected dentin surfaces, at the expense of both amorphous and crystalline new mineral.

Attained nanohardness and Young's modulus is displayed in Table 2. Raman spectroscopy through single point spectra results are shown in Tables 3 and 4. Raman spectra of sound and caries-affected dentin untreated and after Zn-free and Zn-

containing amalgams removal are reflected in Figures 1 and 2, respectively. Fibrils width (nm) at sound and caries-affected dentin surfaces, untreated, Zn-free and Zn-containing amalgams, are read in Figure 3. AFM images of caries-affected dentin surface untreated, or after restoring with Zn-free and Zn-containing amalgams are shown in Figure 4.

The present research sought to gain insights into the role of different Zn-free or Zn-containing amalgams leading to mechanical recovery and remineralization of partially demineralized tissue in caries-affected dentin substrata. These studies were based on both chemical and mechanical heterogeneity of the peritubular and intertubular dentin. Dentin is a composite of collagen molecules and nanocrystals of hydroxyapatite. Akin to bone[36], it derives its mechanical behavior from the collective contributions of these elements and their structural arrangements over length scales ranging from the nano- to the microscale[37]. Nanoindentation is the most commonly applied means of testing the mechanical properties of materials or substrates[38]. Due to the increase in mineral content of dentin after amalgam placement[20], changes to the nanomechanical behavior are not unexpected. Kinney *et al*. (1999)[39] obtained 28.6 GPa of elasticity modulus at sound peritubular dentin, which resulted closer to our present results (29.7 GPa) (Table 2) but lower than data published by Balooch *et al*. (2001)[40], probably because testing by Balooch was performed in dry conditions. At peritubular dentin, nano-hardness (Hi) and Young's modulus (Ei) values did not change in caries-affected dentin substrata after amalgam restorations, except when Zn-free amalgams were employed, that showed the lowest Hi values. Neither Hi or Ei at peritubular dentin changed when caries-affected dentin was submitted to restoration, though Zn-containing amalgams reduced both nanomechanical properties when sound dentin was treated. Anyhow, it can be assumed that peritubular dentin did not induce significant changes in overall mechanical properties of the dentin, after analyzing the present outcomes (Table 2), and in agreement with Kinney *et al.* (1999)[39].

In general, Hi and Ei were higher at intertubular sound dentin than at caries-affected dentin, as reported by Marshall *et al.* (2001)[41,42], except when Zn-containing amalgams were employed and Ei was measured, that resulted similar in both groups (Table 2). Nevertheless, intertubular dentin is expected to have a modulus gradient from 2.7 GPa at the untreated caries-affected dentin, ramping up to 18.85 GPa after removal of Zn-containing restorations from the carious substrate, lower that at sound dentin (25.4 GPa), due to the partial demineralization[43].This rise in nanomechanical properties correlates with an augmentation of bands at 430 (56.04) and 451 (54.82) cm^{-1} (v_2 mode) (~30 and 43% increase, respectively), assigned to vibration of carbonate calcium phosphate in apatite lattice[27] in carious dentin, after Zn-containing amalgam removal, in comparison with the untreated dentin (39.27 and 30.65, respectively) (Table 3) (Fig. 2A).

The phosphate stretching vibrational bands are always used to monitor the formation of mineral deposits[44], in which the prominent peaks in the region from 400 to 1100 cm^{-1} represent vibration of the v_1-v_4 phosphate of hydroxyapatite (HAp). The typical Raman spectrum of HAp reference sample gives rise to a sharp and major peak at 959 cm^{-1} arising from the symmetric stretching vibration of v_1 PO_4^{3-}[45]. The improvement in dentin mineralization correlates with augmentation at v_4 asymmetric bending mode PO_4^{3-}, at 579 cm^{-1} peak, which attained lower difference of intensities between the caries-affected dentin and the sound dentin spectra after removing the Zn-containing amalgams (5.16 cm^{-1}) making them more similar, in comparison with the untreated group (56.71 cm^{-1}) (Fig. 2B), confirming healing of the substrate[5], *i.e*., remineralization of dentin (Table 3). It is important to emphasize that amorphous Ca/P

provides a local ion-rich environment which is considered favorable for *in situ* generation of prenucleation clusters, succeeding further dentin remineralization[46]. On the other hand, the shift intensity at 590 cm^{-1} peak, additional expression of PO_4^{3-} v_4, augmented in the same group (caries-affected dentin treated with Zn-containing amalgam). This controversial data requires further research. Similarly, peaks at 1023, 1043, 1052 cm^{-1} (asymmetric stretching v_3 mode of phosphate PO_4^{3-}) increase in the caries spectrum[5] (Table 3), but diminished in the present research when both Zn-free (Fig. 1A) and Zn-containing amalgams were used, demonstrating dentin remineralization[47]. This higher presence of minerals complied with a drop in the bacterial metabolic activity and organic content detected at the carious tissue after removal of both kind of amalgam restorations, as was reflected in Table 3 and Fig. 2C, by the decrease in fluoridated apatite (peak at 575 cm^{-1})[32]. The lack of augmentation (in caries-affected dentin treated with Zn-free amalgams) or the discrete growth (in caries-affected dentin treated with Zn-containing amalgams) of 579/959, 1043/959 and 1069/959 (Table 3) makes sure that the caries-affected tissue is decreasing as result of dentin remineralization[5]. Images of specimens remineralized after removal of Zn-containing amalgam revealed fibrillar structures with significant topographical changes that suggest a preferential organization of mineral within the surface of collagen fibrils, in an intrafibrillar manner[48]. The remineralization procedure made the fibrils to exhibit a growing width of 73.05 nm (Figs. 3, 4C), and under higher magnification, the prototypical 67-nm-D-periodicity banding of collagen fibrils[49]was observed. This typical staggered pattern of collagen fibrils was not visible in the partially demineralized dentin of untreated caries-affected dentin (Fig. 4A), but was evident when this substrate became clearly remineralized (Fig. 4C·II). This finding is consistent with fibrils containing intrafibrillar and extrafibrillar mineral[49,50].

Collagen regulates mineralization, and a single mutation on a gen that encodes for an α-chain can be responsible for osteogenesis imperfect and dentinogenesis imperfect type I[34]. Proline and hydroxyproline represent about 10% of the total collagen, *i.e.* 2% of the tooth[24]. They are essential aminoacid marker for the presence of collagen[2].Raman bands corresponding to proline (855 cm^{-1}) and hydroxyproline (871 cm^{-1}) showed higher intensity peaks in caries-affected dentin than in sound substrata treated with amalgam, in comparison with the untreated samples (Table 4) (Figs. 2D and 1B). Differences between sound dentin and caries-affected dentin were lower after amalgam restoration than before restoration (Table 4), indicating marked changes in the structure of collagen[45] and making both substrata similar. Those closer differences were also attained after measuring the intensity peak at *i)* 920 cm^{-1} (Table 4), assigned to P-OH stretching and the ν(C-C) of hydroxylated proline. The prolyl-hydroxylase notably increases the structural stability of collagen, as the hydroxylation of the proline aminoacid is an important biochemical process for maintaining the connective tissue of higher organisms[22,33]*;* and *ii)* the Raman peaks at both 937 cm^{-1} and 1001 cm^{-1}, indicatives of proline/hydroxyproline/C-C and phenylalanine, respectively[23]. Differences were markedly reduced when Zn-contained amalgams were used in comparison with samples treated with Zn-free restorations (Table 4) (Fig. 2D).

The amide I band is representative of the secondary structure of proteins. Peak at 1620 cm^{-1} is attributed to the amide I feature of dentin and hydrated gel-like collagen. The frequency of this feature, which corresponds to the spectral peak that is assigned to the Y8a tyrosine side chain of solution-phase collagen[32], augmented in both untreated (~1.49 fold) and specimens treated with Zn-containing amalgams (~1.04 fold), when sound and caries-effected dentin were compared (Table 4). Therefore, an improvement of the structural treated dentin which is typically recognized by specific helical

polypeptide back bone torsion angles and specific main chain hydrogen bond pairings, is expected. This difference also denotes a greater sensitivity to molecular orientation in order to enhance further crystallization. From a clinical standpoint, recovery[51], better organization[52], and collagen quality[53] may be inferred. In general, amide I at 1637 cm^{-1} ($C_1O_1…H_2O$), 1662 cm^{-1} ($C_2O_2…H_4N_4$) and 1694 cm^{-1} (C3O3… H_2O)[34] followed similar trend (Table 4). The amide A band, at 3396 cm^{-1} showed a 2.15 cm^{-1} (sound dentin) and 7.05 cm^{-1} (caries-affected dentin) shift to high frequencies, respectively, when Zn-containing amalgams were employed (Table 4). Similar trend was followed at 3388 cm^{-1} (Fig. 2E). The amide A frequency shift indicated that NH groups were involved in a new set of hydrogen bonds of weaker strength[34]. The amide B shift to low frequencies (Table 4) also was representative of weaker interactions. Total water content increased, as suggested by the rise of the 3420 cm^{-1} shoulder[34], indicating that water associated with other constituents is gained during remineralization, probably due to displacement of the collagen fibrils caused by interfibrillar crystal deposition[54].

Band peak at 1062 cm^{-1} increased at both sound dentin and caries-affected dentin after restoring with Zn-containing amalgams (Fig. 2F). This signal corresponds to proteoglycans, which form a multifaceted scaffold system with attached amorphous macromolecules, possibly lipids and other proteolipids complexes, that provides support and facilitates formation of new mineral[2]. This hypothesis was confirmed in the present research, as intensity peaks at 1448 cm^{-1} and 1656 cm^{-1}, corresponding to lipids and proteins, arose an average of ~1.36 and ~1.31 fold, in sound and caries-affected dentin, respectively, after treating with Zn-containing restorations (Table 4) (Fig. 2G). *Lamina limitants* is an electro-dense, sheet-like structure that lines the entire length of demineralized dentin tubules and is mainly composed of glycosaminoglycans and proteoglycan protein cores[2]. Proteoglycans and glycosaminoglycans (or shape modulus complexes-lipids and proteolipids) participate in biomineralization via the action of the highly negatively charged glycosaminoglycan side chains in recruiting and stabilizing positively charged calcium ions, conducting a biological signaling role[2]. This function would be involved in the signaling mechanisms that activate the odontoblast response during dentin remineralization, in disease[2,41,55].

Dentin remineralization has been achieved after submitting the caries affected dentin substrata to Zn-containing amalgam restorations and thermocycling, as stated above. To determine the nature of this new mineral poses the next challenge. The dentin organic matrix regulates crystal growth and multiplication; the results reported here suggest that it also may influence crystal maturation. The phosphate ν_1 band at 950 and 956 cm^{-1}, characteristic of amorphous calcium phosphate[5,27] shifter to a more lower value, ~12.5 and 18.4% respectively, in comparison with the untreated dentin when caries-affected dentin was Zn-containing amalgam treated and thermocycled (Fig. 2D); the rest of the ν_1 modes followed the same trend (Table 3). Similarly, this drop was accompanied by a lower marker for calcification (lower 954 cm^{-1} peak)[23]. As a consequence, active dentin remodeling did not occur at the new substrate (lower 1003 cm^{-1} peak)[27], resulting a lower stoichiometric HAp (decrease of 963 cm^{-1} peak)[27] with decreased maturity. In addition, amorphous-like apatite species (956 cm^{-1})[27] diminished at the interface of caries-affected dentin treated with Zn-containing amalgams, affecting the nanomechanical properties at the dentin surface (Table 2).

Since an early event of demineralization is the dissolution of CO_3^{2-} by acid attack, one might expect the spectra of carious lesions to have an increase of ν_1 PO_4^{3-} Raman shift at 959 cm^{-1}[5], but such change was neither observed in this group, as appointed before, since this intensity peak became ~17% reduced after removing the Zn-containing amalgam (Table 3) (Fig. 2B). These findings reveal the presence of lower

degrees of impurities or crystal imperfections and amorphous components, with increased chemical stability[56], and creates biogenic apatites that are characterized by a relative degree of crystallinity[57] and non-stoichiometry, as referred the rest of the v_1 modes, which followed the same trend (Table 3). Remineralization is a dynamic process in which amorphous phase formation, phase stabilization, and transition of calcium phosphate continuously occur[44]. It begins as calcium phosphate nidus, made of hydroxyapatite, whitlockite, brushite and ocatcalcium phosphate[58] and progresses to HAp crystal formation within the collagen matrix[45]. We speculate that zinc may have acted as crystal growth inhibitor facilitating amorphous calcium phosphate stabilization, intrafibrillar mineralization of collagen, and the ensuing increase of mechanical properties[59,60] (Table 2). It may be observed that in the v_1 spectral region (1000-900 cm^{-1}), Raman spectra always contain detailed band peaks with a relative narrow line width (<12 cm^{-1} full width at half maximum for the major peaks)[32], in the untreated samples. It also may be observed that these bands are weaker in intensity and wider after treating the caries-affected dentin with both Zn-free (Fig. 1) and Zn-containing amalgam restorations (Fig. 2D). This indicates the presence of amorphous phosphate-based minerals in dentin. As the mineral became less perfect, the mineral lattice had excessive vacancies and/or substitutions, and a decreased crystalline-to-amorphous ratio[61], with shift bands showing lower wavenumbers and broadens[27]. Different phosphate v_1 spectral components have been attributed to different mineral species that compose the substrate[27], and other substitution (HPO_4^{2-}, CO_3^{2-}, in place of an OH^- (A-type carbonate), Cl^-, and or F^-[27] which create crystal disorder hindering the ability of biological apatites to carry out their tissue-specific functions[62]. It may be that the energy generated from the propagation of the thermal stress causes the mineral to undergo a phase transformation and amorphization as is commonly seen in geological and synthetic apatites[27].

When the Zn-containing amalgams were removed from the caries-affected dentin surfaces, bands at 430 and 451 cm^{-1} (PO_4^{3-} v_2 mode), assigned to vibration of carbonate calcium phosphate in apatite lattice[27], increased (~30 and 43%, respectively) when compared with the untreated group of dentin (Table 3) (Fig. 2A). It has been previously reported that the incorporation of carbonate, expressed as augmentation of the relative mineral concentration and the gradient in mineral content (carbonate/phosphate), deforms the crystal structure[5,63] causing a decrease in crystallynity[61], as confirmed the drop of the ratio 1020/1030 (Table 3) as a result of the decrease of non-stoichiometric apatites containing HPO_4^{2-}, CO_3^{2-}, and vacancies and increase of stoichiometric apatites at 1030 cm^{-1}[34]. Dentin is primarily a nonstoichiometric carbonated hydroxyapatite lattice. Carbonate typically substitutes into the lattice for PO_4^{3-} (B-type carbonate)[27], whose concentration, therefore, augments at the dentin substrate, as was confirmed after the increase (~5%) at 1069 cm^{-1} peak (type-B CO_3^{2-}), and (~38.8%) at1104 cm^{-1} peak (type-A CO_3^{2-})[32] (Fig. 2D). Nevertheless, the intensity peak at 1072 cm^{-1} decreased similarly in the same group, confirming the lack of significance of both signals when sound and carious dentin were evaluated[5] (Fig. 2D). The increase of the symmetric bending mode (v_2) PO_4^{3-} was also unveiled through the augmentation of bands at 431 and 446 cm^{-1}[5]. Even more, Ko *et al.* (2005)[5] determined higher intensity values at 431 than at 446 cm^{-1} in caries-affected dentin spectra (Fig. 2A). This relationship comply with the values that were reported in the untreated group of the present research, and resulted practically similar after submitting the caries affected dentin surfaces to Zn-containing amalgam restoration (Table 3), *ie.*, 56.04 (431 cm^{-1}) *vs* 56.62 (446 cm^{-1}), respectively. Nevertheless, it is worth to emphasize that the enhanced mineralization of caries-affected dentin was also

attained at the expenses of increased crystallinity as it was corroborated after the augmentation of *i)* the intensity peak at 1145 cm^{-1} that indicated maturation linked to the loss of HPO_4^{2-}, and *ii)* R1090/1125, 1090/1115, and 1090/1100 (Table 3)[34].

These are, to the best of our knowledge, the only available results from nano-mechanical properties and single-point Raman spectroscopy experiments submitted to amalgam restorations. The association between the increase of mechanical properties and remineralization at the carious dentin after having been influenced by Zn was reliably demonstrated. Therefore, the null hypothesis that there are no differences in dentin mineralization, expressed in terms of mechanical and chemical properties of sound and caries-affected substrata after removal of Zn-free *vs* Zn-containing amalgam restorations, must be rejected. Ko *et al*. (2005)[5] hold that spectral differences between sound and carious enamel arise from structural characteristics of the enamel rods. We assume that those spectral differences detected between caries-affected dentin untreated and restored with Zn-containing amalgams lies, partially, in the crystallite structural orientation changes promoted by the presence of zinc. For this reason, further additional research should be implemented, in order to determine if the present findings are or not supported on changes of crystallinity, crystallite size, grain size and texture between sound and carious dentin. Thereby, the lack of transmission electron microscopy (TEM) and X-ray diffraction (XRD) analyses that represents a limitation of our study, needs to be highlighted and performed in future actions.

Conclusions

Zn-containing amalgam restorations remineralized the partially mineral-depleted substratum in caries-affected dentin surfaces, at the expense of both amorphous and crystalline new mineral. The crystalline mineral will provide high mechanical properties, chemical stability and lower values of sorption and solubility to the dentin, *i.e.*, low biodegradability. On the contrary, the amorphous calcium phosphate provides a local ion-rich environment which is considered favorable for *in situ* generation of prenucleation clusters, succeeding further dentin remineralization. Furthermore, if crystalline calcium phosphates are formed, they will have long degradation times, requiring months or even years to provide ions to the remineralizing media. We eventually concluded that the crystalline calcium phosphate may render clinical service at short term and that amorphous calcium phosphate may do it at long term.

Acknowledgments

Project MAT2014-52036-P supported by the Ministry of Economy and Competitiveness (MINECO) and European Regional Development Fund (FEDER).
The authors have no financial affiliation or involvement with any commercial organization with direct financial interest in the materials discussed in this manuscript. Any other potential conflict of interest is disclosed.

References

[1] M. Kay, R.A. Young, A.S. Posner, *Nature* **1964,** *12*, 1050.
[2] L.E. Bertassoni, K. Stankoska, M.V. Swain, *Micron* **2012,** *43*, 229.
[3] K. Stankoska, L. Sarram, S. Smith S, A.K. Bedran-Russo, C.B. Little, M.V. Swain, L.E. Bertassoni, *Aust. Dent. J.* **2015,** *5* [Epub ahead of print].
[4] S. Habelitz, M. Balooch, S.J. Marshall, G. Balooch, G.W. Marshall Jr, *J. Struct. Biol.* **2002**, *138*, 227.
[5] A.C. Ko, L.P. Choo-Smith, M. Hewko, L. Leonardi, M.G. Sowa, C.C.S. Dong, P. Williams, B. Cleghorn, *J. Biomed. Opt.* **2005,** *10*, 031118.
[6] L. Zheng, J.F. Hilton, S. Habelitz, S.J. Marshall, G.W. Marshall, *Eur. J. Oral Sci.* **2003***, 111*, 243.
[7] M. Yoshiyama, F.R. Tay, Y. Torii, Y. Nishitani, J. Doi, K. Itou, B. Ciucchi, D.H. Pashley, *Am. J. Dent.* **2003**, *16*, 47.
[8] T.F. Watson, A.R. Atmeh, S. Sajini, R.J. Cook, F. Festy, *Dent. Mater.* **2014**, *30*, 50.
[9] S.K. Makhija, V.V. Gordan, G.H. Gilbert, M.S. Litaker, D.B. Rindal, D.J. Pihlstrom, V. Qvist, *J. Am. Dent. Assoc.* **2011**, *142*, 622.
[10] K. Lyons; Ministry of Health, *N. Z. Dent. J.* **2003**, *99*, 10.
[11] M.G. Rasines Alcaraz, A. Veitz-Keenan, P. Sahrmann, P.R. Schmidlin, D. Davis, Iheozor-Ejiofor, *Cochrane Database Syst. Rev*. **2014**, *31,* CD005620.
[12] FDA (US Food and Drug Administration), **2013,** http://www.fda.gov/MedicalDevices/ProductsandMedicalProcedures/DentalProducts/DentalAmalgam/ucm171094.htm.
[13] ADA (American Dental Association), **2013**, http://www.ada.org/1741.aspx.
[14] M. Toledano, F.S. Aguilera, E. Osorio, M.T. López-López, I. Cabello, M. Toledano-Osorio, R. Osorio, *Biointerphases* **2015**, *10*, 041004.
[15] J.L Ferracane, *Dent. Mater.* **2013**, *29***,** 51.
[16] A.R. Hunter, E.T. Treasure, A.J. Hunter, *Oper. Dent.* **1995**, *20*, 2.
[17] P. Spencer, Q. Ye, A. Misra, S.E. Goncalves, J.S. Laurence, *J. Dent. Res*. **2014**, *93*, 1243.
[18] J.D. Scholtanus, W. van der Hoorn, M. Ozcan, M.C. Huysmans, J.F. Roeters, C.J. Kleverlaan, A.J. Feilzer, *Am. J. Dent*. **2013**, *26*, 185.
[19] J.F. McCabe, A.W.G. Walls, *Applied Dental Materials 9th Edition,* Wiley-Blackwell, Oxford, **2008**.
[20] M. Toledano, E. Osorio, F.S. Aguilera, I. Cabello, M. Toledano-Osorio, M.T. López-López, R. Osorio, *Optimizing nano-dynamic mechanical and micro-Raman analyses for high resolution, in amalgam-restored dentin surfaces submitted to thermocycling*, *Microsc. Microanal.* **2015**. *In press.*
[21] T.M. Wilkinson, S. Zargari, M. Prasad, C.E. Packard, *J. Mater. Sci*. **2015**, *50*, 1041.
[22] J.H. Kinney, M, Balooch, S.J. Marshall, G.W. Marshall Jr., T.P. Weihs, *Arch. Oral Biol.* **1996***, 41*, 9.
[23] A. Kunstar, J. Leijten, S. van Leuveren, J. Hilderink, C. Otto, C.A. van Blitterswijk, M. Karperien, A.A. van Apeldoorn, *J. Biomed. Opt.* **2012**, *17*, 116012.
[24] S.Moreno-Flores, J.L. Toca-Herrera, *Hybridizing surfaces probe microscopies. Toward a full description of the Meso- and Nanoworlds*, CRC Press, Taylor & Francis Group, Florida, USA, **2013**.
[25] R.Z. LeGeros, R. Kijkowska, C. Bautista, J.P. LeGeros, *Connect. Tissue Res*. **1995**, *33*, 203.
[26] T. Saito, A.L. Arsenault, M. Yamauchi, Y. Kuboki, M.A. Crenshaw, *Bone* **1997**, *21*, 305.

[27] J.A. Timlin, A. Carden, M.D. Morris, R.M. Rajachar, D.H. Kohn, *Anal. Chem*. **2000**, *72*, 2229.
[28] M. Özcan, G. Pekkan, *Oper. Dent*. **2013**, *38*, 63.
[29] A. Saracoglu, M. Ozcan, O. Kumbuloglu, M.Turkun, *Oper Dent*. **2011**, *36*, 545.
[30] L. Han, A.J. Grodzinsky, C. Ortiz, *Annu. Rev. Mater. Res.* **2011,** *1*, 133.
[31] W.C. Oliver, G.M. Pharr, *J. Mater. Res*. **1992**, *7,* 1564.
[32] R. Ramakrishnaiah, G. urRehman, S. Basavarajappa, A.A. Al Khuraif, B.H. Durgesh, A.S. Khan, I. urRehman, *Appl. Spectrosc. Rev.* **2015**, *50*, 332.
[33] J.C. Garcia-Guinea, A.C. Jorge, L. Tormo, M. Furio, E. Crespo-Feo, V. Correcher, P. Prado-Herrero, A.C. Soria, J. Sanz, J.L. Nieves-Aldrey, *Sci. World J.* **2011**, *18*, 186.
[34] D. Magne, P. Weiss, J.M. Bouler, O. Laboux, G. Daculsi, *J. Bone Miner. Res.* **2001**, *16*, 750.
[35] M.T. Kirchner, H.G.M. Edwards, D. Lucy, A.M. Pollard, *J. Raman Spectrosc*. **1997**, *28*, 171.
[36] P. Fratzl, H.S. Gupta, E.P. Paschalis, P. Roschger, *J. Mater. Chem*. **2004**, *14*, 2115.
[37] J.H. Kinney, R.K. Nalla, J.A. Pople, T.M. Breunig, R.O. Ritchie, *Biomaterials* **2005**, *26*, 3363.
[38] B. Poon, D. Rittel, G. Ravichandran, *Int. J. Solids Struct*. **2008**, *45*, 6018.
[39] J.H. Kinney, M. Balooch, G.W. Marshall, S.J. Marshall, *Arch. Oral Biol.* **1999***, 44*, 813.
[40] M. Balooch, S.G. Demos, J.H. Kinney, G.W. Marshall, G. Balooch, S.J. Marshall, *J. Mater. Sci. Mater. Med.* **2001**, *12*, 507.
[41] J.H. Kinney, G.W. Marshall, S.J. Marshall., *Scanning Microsc*. **1994**, *8*, 197.
[42] G.W. Marshall, S. Habelitz, R. Gallagher, M. Balooch, G. Balooch, S.J. Marshall, *J. Dent. Res.* **2001**, *80*, 1768.
[43] A. Misra, P. Spencer, O. Marangos, Y. Wang, J.L.Katz, *J. R. Soc. Interface* **2005**, *22*, 145.
[44] P. Tramini, B. Pélissier, J. Valcarcel, B. Bonnet, L. Maury, *Caries Res*. **2000**, *34,* 233.
[45] W.T. Cheng, M.T. Liu, H.N. Liu, S.Y. Lin, *Microsc. Res. Tech*. **2005**, *68*, 75.
[46] Y. Liu, L. Tjäderhane, L. Breschi, A. Mazzoni, N. Li, J. Mao, D.H. Pashley, F.R. Tay, *J. Dent Res*. **2011**, *90*, 953.
[47] B. Mohanty, D. Dadlani, D. Mahoney, A.B. Mann, *Caries Res*. **2013**, *47*, 27.
[48] D.S. Kim, J. Kim, K.K. Choi, S.Y. Kim, *J. Dent*. **2011**, *39*, 855.
[49] K.M. Zurick, C. Qin, M.T. Bernards, *J. Biomed. Mater. Res. A.* **2013,** *101*, 1571.
[50] L.E. Bertassoni, S. Habelitz, M. Pugach, P.C. Soares, S.J. Marshall, G.W. Marshall Jr, *Scanning* **2010,** *32*, 312.
[51] C. Xu, Y. Wang, *J. Adhes. Dent.* **2012,** *14*, 11.
[52] M. Toledano, F.S. Aguilera, S. Sauro, I. Cabello, E. Osorio, R. Osorio, *Dent. Mater.* **2014**, *30*, e169.
[53] H. Salehi, E. Terrer, I. Panayotov, B. Levallois, B. Jacquot, H. Tassery, F. Cuisinier, *J. Biophotonics* **2013***,6*, 765.
[54] L.C. Bonar, S. Lees, H.A. Mook, *J. Mol. Biol*. **1985**, *181*, 265.
[55] R.M. Farahani, K.A. Nguyen, M. Simonian, N. Hunter, *Am. J. Pathol.* **2010**, *177*, 1901.
[56] A. Moshaverinia, S. Ansari, M. Moshaverinia, N. Roohpour, J.A. Darr, I. Rehman, *Acta Biomater.* **2008**, *4*, 432.
[57] A. Bigi, E. Boanini, M. Gazzano, K. Rubini, P. Torricelli, *Biomed. Mater. Eng*. **2004**, *14*, 573.

[58] C. Kato, M. Suzuki, K. Shinkai, Y. Katoh, *Dent. Mater. J.* **2011**, *30*, 583.
[59] I.M. Low, *J. Am. Ceram. Soc*. **2004**, *87*, 2125.
[60] M. Toledano, F.S. Aguilera, E. Osorio, I. Cabello, M. Toledano-Osorio, R. Osorio, *Biointerphases* **2015,** *10*, 031002.
[61] M. Toledano, F.S. Aguilera, M.T. López-López, E. Osorio, I. Cabello, M. Toledano-Osorio, R. Osorio, *XRD crystal-lattice characterisation of biogenic apatites on human dentine submitted to amalgam restorations*, *J. Mech. Behav. Biomed.* **2015**. *In press*.
[62] J.D. Pasteris, B. Wopenka, J.J. Freeman, K. Rogers, E. Valsami-Jones, J.A. van der Houwen, M.J. Silva, *Biomaterials* **2004**, *25*, 229.
[63] P.G. Spizzirri, N.J. Cochrane, S. Prawer, E.C. Reynolds, *Caries Res*. **2012**, *46*, 353.

Legends of figures

Figure 1. Average Raman spectra of sound and caries-affected dentin untreated and after Zn-free amalgam removal, in the region from 400 to 3500 cm^{-1}. **A**, Truncated Raman spectrum in the region from the asymmetric stretching v_3 mode of phosphate PO_4^{3-}, from 1000 to 1100 cm^{-1}. **B**, Truncated Raman spectrum in the region from the proline and hidroxyproline (855 cm^{-1}, 871 cm^{-1}), from 800 to 900 cm^{-1}.

Figure 2. Average Raman spectra of sound and caries-affected dentin untreated and after Zn-containing amalgam removal, in the region from 400 to 3500 cm^{-1}. **A**, Truncated Raman spectrum from the carbonated calcium phosphate in the apatite lattice, in the region from 440 to 500 cm^{-1}. **B**, Truncated Raman spectrum from the phosphate PO_4^{3-}, at 959 cm^{-1}($v_1$mode), from 900 to 1000 cm^{-1}. **C**, Truncated Raman spectrum from the fluoridated apatite, and $PO_4^{3-}v_4$, from 550 to 600 cm^{-1}. **D**, Truncated Raman spectrum from the proline and hidroxyproline (855 cm^{-1}, 871 cm^{-1}), collagen (937 cm^{-1}), amorphous-like apatite species (956 cm^{-1}), phenylalanine (1001 cm^{-1}), B-type carbonate CO_3^{2-} (1069 cm^{-1} and 1072 cm^{-1}), and A-type carbonate CO_3^{2-} (1104 cm^{-1}), from 800 to 1150 cm^{-1}. **E**, Truncated Raman spectrum from Amide A (3388 cm^{-1} and 3396 cm^{-1}), from 3300 to 3400 cm^{-1}. **F**, Truncated Raman spectrum from proteoglycans (1062 cm^{-1}), from 1000 to 1100 cm^{-1}. **G**, Truncated Raman spectrum from lipids and proteins (1448 cm^{-1} and 1656 cm^{-1}), from 1400 to 1700 cm^{-1}.

Figure 3. Mean and standard deviation of fibrils width (nm) at sound and caries-affected dentin surfaces, untreated and treated with Zn-free or Zn-containing amalgams. Identical lowercases indicate no significant differences at sound dentin; identical capital letters indicate no significant differences at caries affected dentin.* indicates differences between SD and CAD. Abbreviations: SD: sound dentin, CAD: caries-affected dentin.

Figure 4. A, AFM images of caries-affected dentin surfaces untreated; **AI**, 2 x 2 μm top-view and surface plot image of partially demineralized collagen fibrils (arrows), limiting mineral-depleted areas (pointers); **AII**, AFM phase image (2 x 2 μm) showing the collagen fibrils (arrows). **B**, AFM images of caries-affected dentin surface restored with Zn-free amalgam. **BI**, 2 x 2 μm top-view and surface plot image of partially remineralized collagen fibrils (arrows) which show some limited mineral-depleted areas (pointers) as well as the entrance of a some tubules (asterisks); **BII**, AFM phase image (2 x 2 μm) showing the bandwidth of the collagen fibrils (arrows). **C**, AFM images of caries-affected dentin surface restored with Zn-containing amalgam; **CI**, 2 x 2 μm top-view and surface plot image of the advanced remineralized collagen fibrils (arrow); **CII**, AFM phase image (2 x 2 μm) showing the wider bandwidth of the collagen fibrils (arrows) and the staggered pattern of collagen fibrils (pointers).

Table 1. Composition of amalgams used in the present study.

AMALGAM	COMPOSITION	
	Alloy powder	**Weight %**
Megalloy EZ®* (Zn-free)	Silver	56.7 %
	Tin	28.6 %
	Copper	14.7%
The recommended alloy to mercury ratio by mass is approximately 1.3:1		
Dispersalloy®* (Zn-containing)	Silver	69 %
	Tin	18 %
	Copper	12 %
	Zinc	1 %
The recommended alloy to mercury ratio by mass is approximately 1:1		

* Dentsply Detrey GmbH Konstanz, Germany.

Table 2. Mean (SD) of nanohardness (GPa) and Young Modulus (GPa) measured at the experimental sound and caries-affected dentin surfaces.

NANO-HARDNESS (Hi)							
Amalgam	**SD**	Means (SD) (GPa)			**CAD**	Means (SD) (GPa)	
Untreated (Without amalgam)	ID	1.0 (0.2)	a	1*	ID	0.3 (0.1)	a 1
	PD	1.6 (0.3)	A	2*	PD	0.8 (0.16)	A 2
Megalloy EZ® (Zn-free)	ID	0.80 (0.11)	a	1*	ID	0.48 (0.06)	b 1
	PD	1.44 (0.41)	B	1*	PD	0.47 (0.07)	B 1
Dispersalloy® (Zn-containing)	ID	0.95 (0.03)	a	1*	ID	0.7 (0.18)	c 1
	PD	0.71(0.31)	B	1	PD	0.77 (0.25)	AB 1
YOUNG MODULUS (Ei)							
Amalgam	**SD**	Means (SD) (GPa)			**CAD**	Means (SD) (GPa)	
Untreated (Without amalgam)	ID	25.4 (3.5)	a	1*	ID	2.7 (0.5)	a 1
	PD	29.7 (0.57)	A	1 *	PD	16.49 (2.11)	A 2
Megalloy EZ® (Zn-free)	ID	22.65 (3.40)	a	1*	ID	16.08 (1.54)	b 1
	PD	33.25 (7.64)	B	1*	PD	15.68 (1.50)	A 1
Dispersalloy® (Zn-containing)	ID	22.48 (0.81)	a	1	ID	18.85 (7.08)	b 1
	PD	19.11 (8.13)	B	1	PD	18.01 (4.66)	A 1

Abbreviations: SD: sound dentin, CAD: caries-affected dentin, ID: intertubular dentin, PD: peritubular dentin. Identical lower cases indicate no differences in intertubular dentin values between the different groups. Identical capital letters indicate no differences in peritubular dentin values between the different groups. Identical numbers indicate no differences between peritubular and intertubular dentin values in the different groups. * indicates differences between sound dentin and CAD at the different substrates.

Table 3. Mineral components in dentin surfaces of untreated teeth and those treated with amalgams.

MINERAL COMPONENTS	Amalgam treatments							
	Untreated		Zn-Free		Untreated		Zn-Containing	
	SD	CAD	SD	CAD	SD	CAD	SD	CAD
v_2 [430-431]	24.01	42.90	39.17	35.25	25.12	39.27	30.94	56.04
v_2 [446]	25.51	34.15	32.56	32.20	20.05	32.10	30.98	56.62
v_2 [451]	24.73	34.94	26.10	33.46	17.51	30.65	25.21	54.82
FA [575]	20.64	33.11	28.35	24.49	18.40	39.90	23.07	34.96
$PO_4^{3-}v_4$ [579]	21.51	32.14	24.25	19.79	20.78	34.93	21.96	33.68
$PO_4^{3-}v_4$ [590]	22.93	38.92	33.51	18.81	21.03	36.08	23.72	50.52
v_1[950]	39.11	55.11	71.64	35.18	43.12	61.33	50.47	54.31
v_1[954]	57.80	102.47	109.88	46.99	63.67	108.19	74.70	72.55
v_1[956]	78.70	119.69	14.80	67.44	84.10	126.44	103.63	103.21
v_1[959]	95.35	145.85	153.84	84.07	91.63	148.34	128.26	123.10
v_1[960]	96.34	146.45	171.95	87.92	102.69	159.59	136.34	130.13
v_1[963]	94.70	142.98	166.77	88.29	101.15	141.86	129.66	122.48
v_1[1003]	6.14	14.61	15.78	7.63	7.59	18.47	8.24	2.87
$PO_4^{3-}v_3$ [1023]	5.85	11.77	17.51	6.63	7.67	15.82	11.48	12.85
$PO_4^{3-}v_3$ [1043]	10.58	21.79	20.22	13.05	11.15	29.30	16.81	27.24
$PO_4^{3-}v_3$ [1052]	9.44	19.45	23.31	13.47	13.56	22.61	16.70	20.25
$CO_3^{2-}v_3$ [1069]	15.32	22.48	34.32	13.42	18.62	23.00	21.36	24.21
$CO_3^{2-}v_3$ [1072]	17.41	20.19	32.63	18.62	19.26	23.79	24.55	22.42
Type A CO_3^{2-} [1104]	7.60	10.44	10.83	4.32	6.03	7.99	9.52	13.05
[1145]	3.47	6.02	6.45	10.61	4.11	5.27	1.48	15.20
R *579/959*	0.23	0.22	0.16	0.24	0.23	0.24	0.17	0.27
R *1043/959*	0.11	0.15	0.13	0.16	0.12	0.20	0.13	0.22
R *1069/959*	0.16	0.15	0.22	0.16	0.20	0.16	0.17	0.20
R *1020/1030*	0.74	0.80	1.15	1.03	0.85	0.95	1.32	0.78
R *1090/1125*	3.50	1.07	1.84	0.77	1.50	0.96	3.07	1.22
R *1090/1115*	2.53	0.73	1.71	1.20	1.33	1.27	6.32	2.73
R *1090/1100*	0.93	0.55	1.25	1.24	1.05	0.88	1.43	3.13

Abbreviations: FA: Fluoridated Apatite; R: Ratio; SD: sound dentin, CAD: caries-affected dentin. Peaks positions are expressed in cm^{-1}.

Table 4. Organic components in dentin surfaces of untreated teeth and those treated with amalgams.

ORGANIC COMPONENTS	Amalgam treatment							
	Untreated		Zn-Free		Untreated		Zn-Containing	
	SD	CAD	SD	CAD	SD	CAD	SD	CAD
C-C proline [855]	10.68	16.76	15.16	12.87	10.40	26.13	10.00	18.35
C-C hydroxyproline[871]	8.19	18.19	11.89	4.03	10.41	22.69	9.79	14.42
C-C hydroxylated proline [920]	8.88	16.38	18.29	12.33	9.16	23.77	9.17	12.81
Collagen [937]	14.72	20.04	26.46	10.71	17.57	26.63	14.92	19.82
Phenylalanine [1001]	6.14	11.15	12.09	8.53	6.83	17.23	7.30	16.18
Proteoglycans [1062]	12.42	25.43	27.50	19.55	13.99	30.78	16.95	32.05
Lipids and proteins CH_2[1448]	18.25	24.06	31.30	28.37	22.34	31.54	28.42	39.34
Lipids and proteins AI [1656]	16.14	22.54	18.97	13.78	18.94	24.42	17.68	20.90
Tyrosine [1610-20]	10.43	15.24	21.41	7.26	14.02	20.87	14.70	15.33
Amide I [1637]	14.89	18.16	20.78	18.11	17.02	32.74	24.69	31.06
Amide I [1662]	14.86	25.42	21.86	19.80	16.80	30.89	23.95	20.70
Amide I [1694]	11.83	18.72	15.33	20.75	13.69	20.14	16.92	18.27
Amide A 3396	4.74	17.58	10.13	10.43	7.23	10.98	9.38	18.03
Amide A 3388	3.12	11.67	3.83	10.09	4.09	12.33	5.51	15.84
Amide B 3078	16.88	8.43	16.71	18.15	22.09	15.07	23.70	8.72
Amide B 3085	12.51	20.90	17.06	23.52	18.52	22.31	20.55	19.79
R Amide I[1694]/960	0.12	0.13	0.09	0.24	0.13	0.13	0.12	0.14
Water content [3420]	5.02	15.18	10.51	6.68	8.79	10.62	6.91	15.17

Abbreviations: R: Ratio; SD: sound dentin, CAD: caries-affected dentin. Peaks positions are expressed in cm^{-1}.

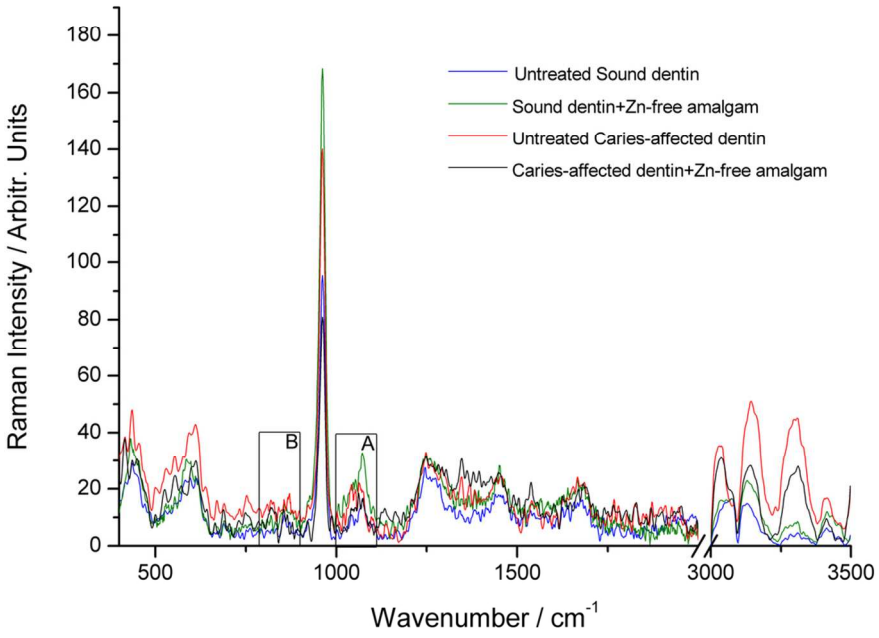

Figure 1. Average Raman spectra of sound and caries-affected dentin untreated and after Zn-free amalgam removal, in the region from 400 to 3500 cm^{-1}
105x78mm (300 x 300 DPI)

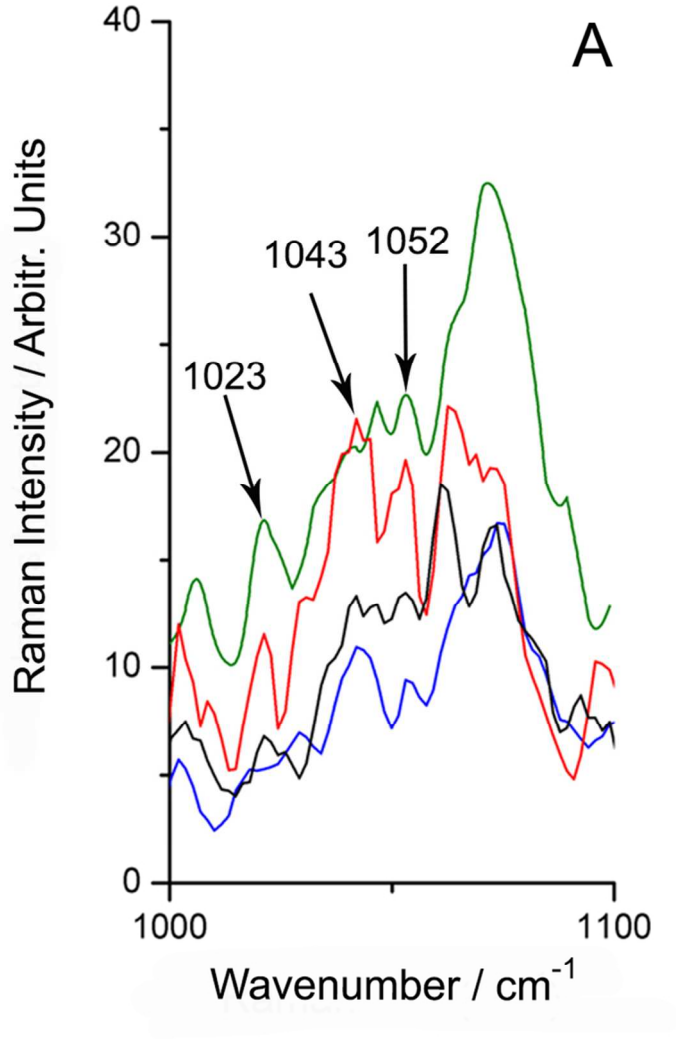

Figure 1A. Truncated Raman spectrum in the region from the asymmetric stretching v_3 mode of phosphate $PO4^{3-}$, from 1000 to 1100 cm^{-1}
69x102mm (300 x 300 DPI)

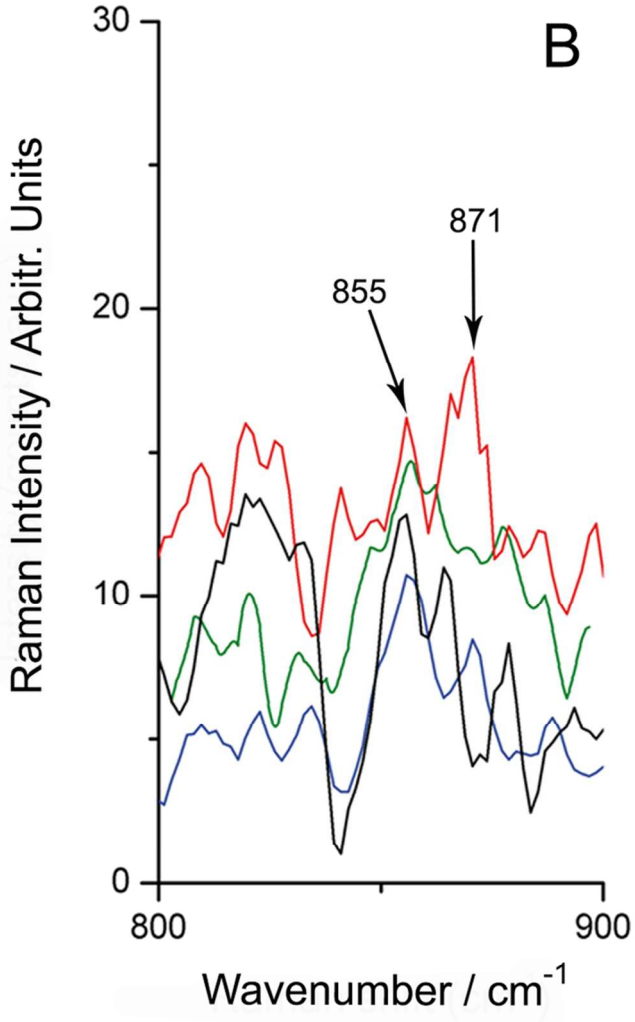

Figure 1B. Truncated Raman spectrum in the region from the proline and hidroxyproline (855 cm^{-1}, 871 cm^{-1}), from 800 to 900 cm^{-1}.
69x102mm (300 x 300 DPI)

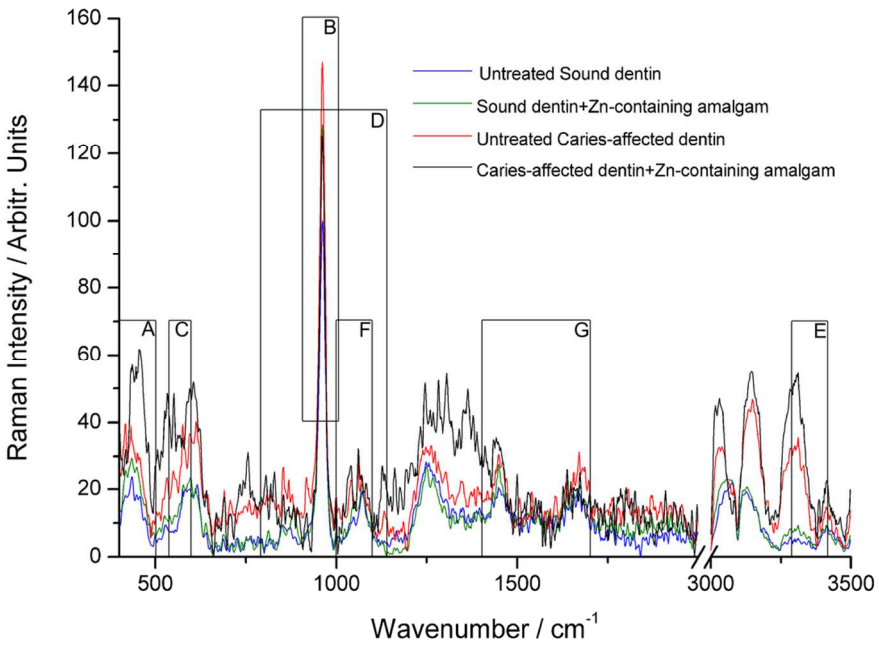

Figure 2. Average Raman spectra of sound and caries-affected dentin untreated and after Zn-containing amalgam removal, in the region from 400 to 3500 cm^{-1}.
105x78mm (300 x 300 DPI)

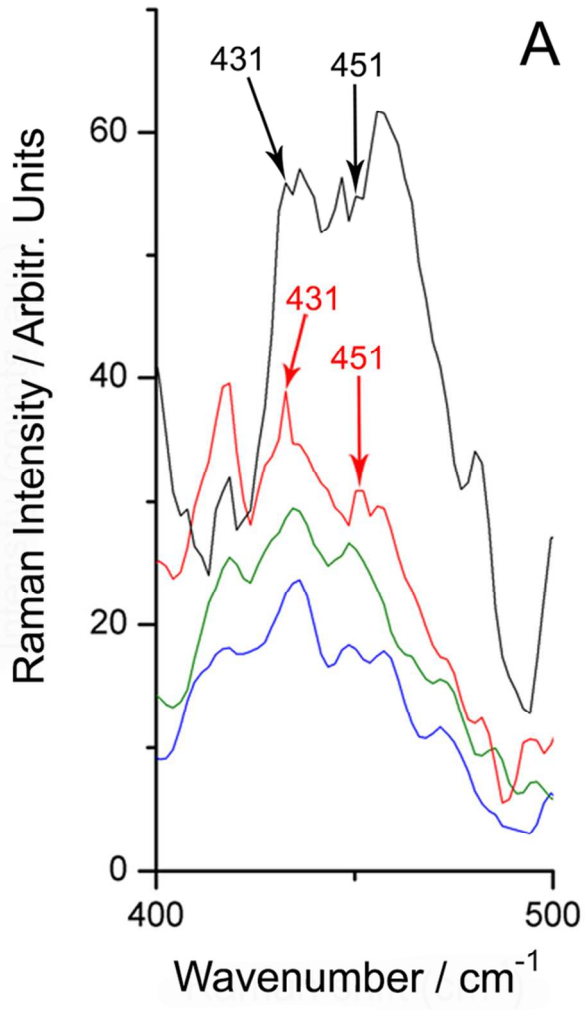

Figure 2A. Truncated Raman spectrum from the carbonated calcium phosphate in the apatite lattice, in the region from 440 to 500 cm^{-1}
69x102mm (300 x 300 DPI)

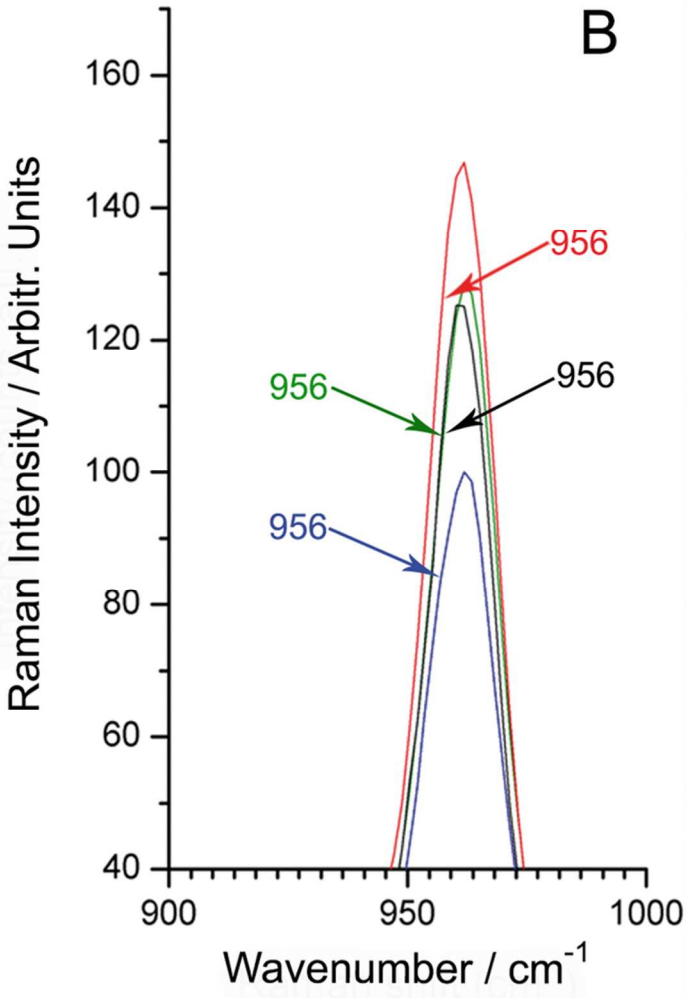

Figure 2B. Truncated Raman spectrum from the phosphate $PO4^{3-}$, at 959 cm^{-1}($v_1$mode), from 900 to 1000 cm^{-1}
69x95mm (300 x 300 DPI)

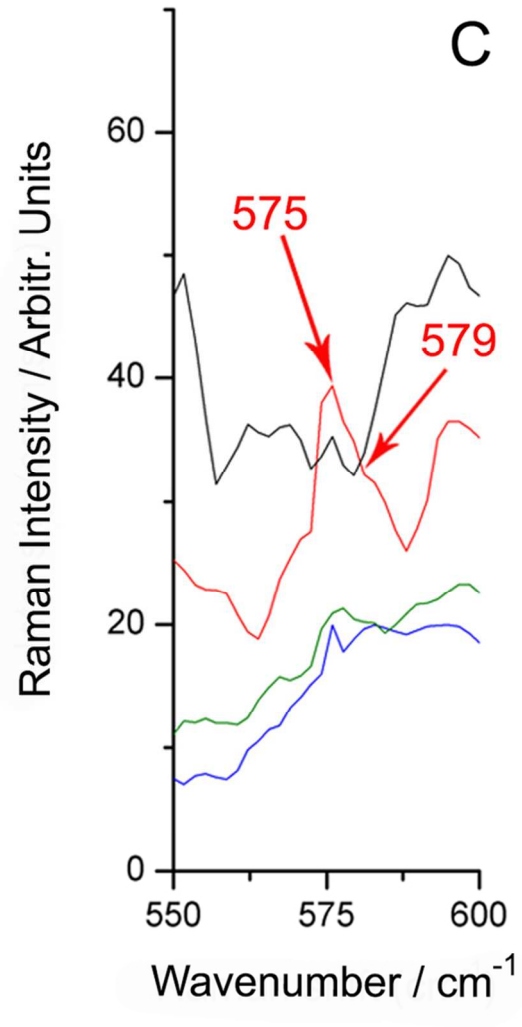

Figure 2C. Truncated Raman spectrum from the fluoridated apatite, and $PO4^{3-}v_4$, from 550 to 600 cm^{-1}
69x102mm (300 x 300 DPI)

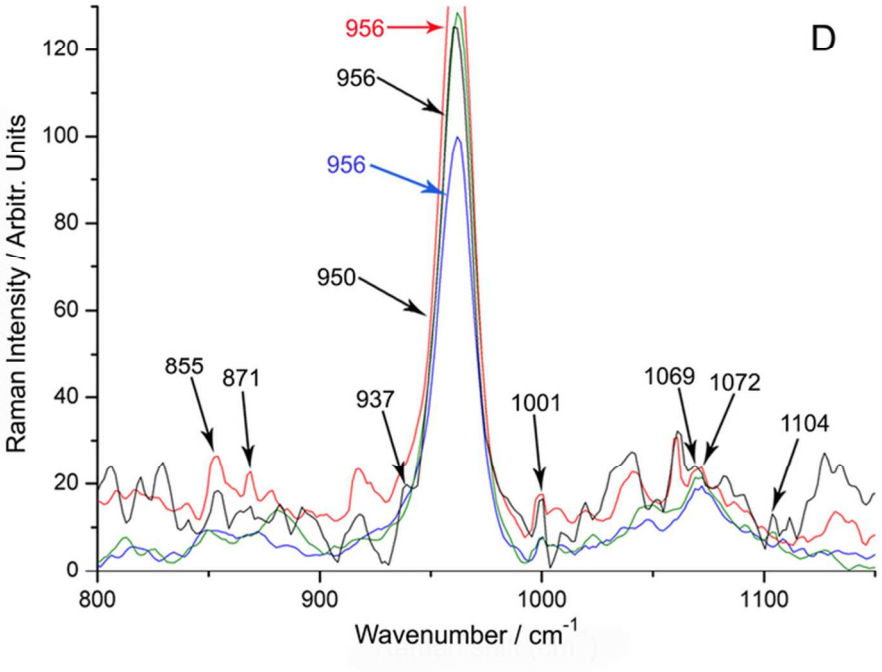

Figure 2D. Truncated Raman spectrum from the proline and hidroxyproline (855 cm^{-1}, 871 cm^{-1}), collagen (937 cm^{-1}), amorphous-like apatite species (956 cm^{-1}), phenylalanine (1001 cm^{-1}), B-type carbonate CO32- (1069 cm-1 and 1072 cm-1), and A-type carbonate CO_3^{2-} (1104 cm^{-1}), from 800 to 1150 cm^{-1}
69x51mm (300 x 300 DPI)

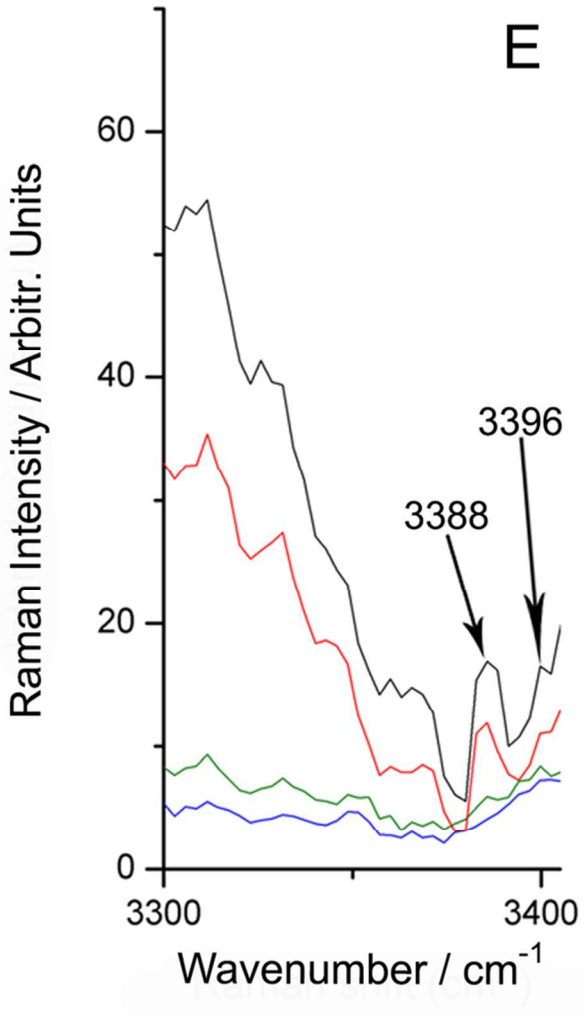

Figure 2E. Truncated Raman spectrum from Amide A (3388 cm^{-1} and 3396 cm^{-1}), from 3300 to 3400 cm^{-1}.
69x95mm (300 x 300 DPI)

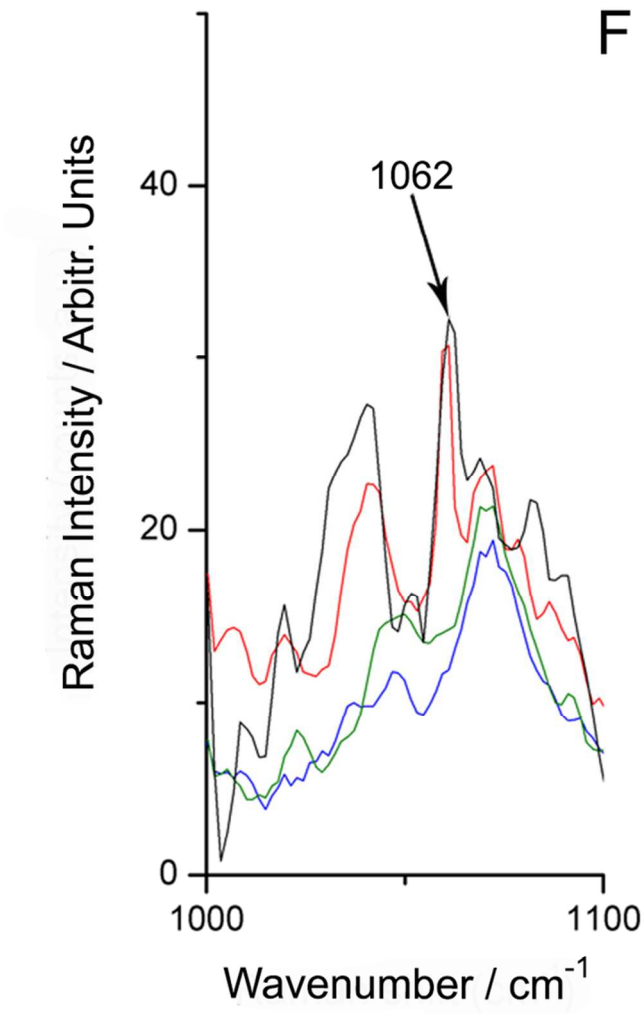

Figure 2F. Truncated Raman spectrum from proteoglycans (1062 cm^{-1}), from 1000 to 1100 cm^{-1}.
69x102mm (300 x 300 DPI)

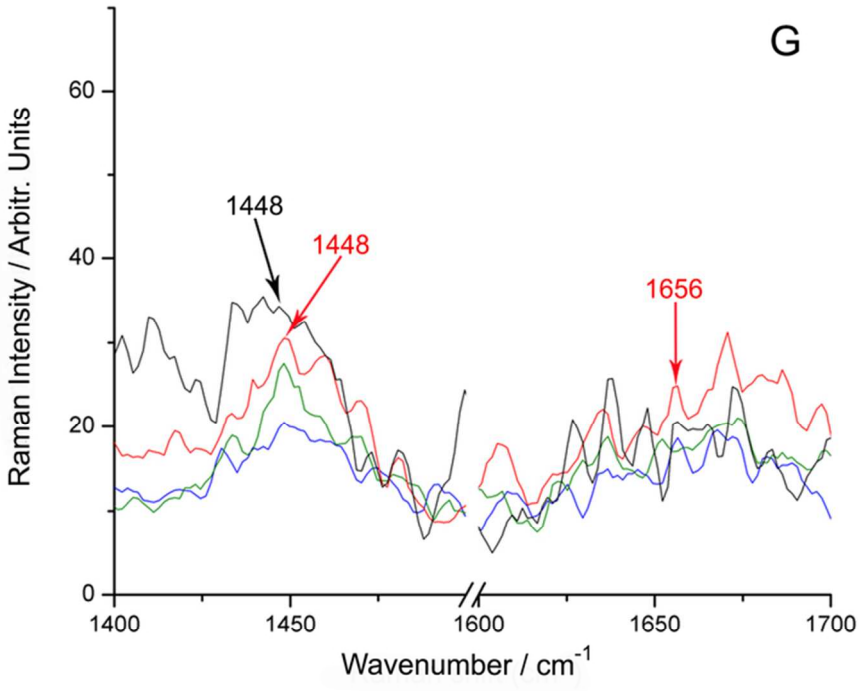

Figure 2G. Truncated Raman spectrum from lipids and proteins (1448 cm^{-1} and 1656 cm^{-1}), from 1400 to 1700 cm^{-1}
69x57mm (300 x 300 DPI)

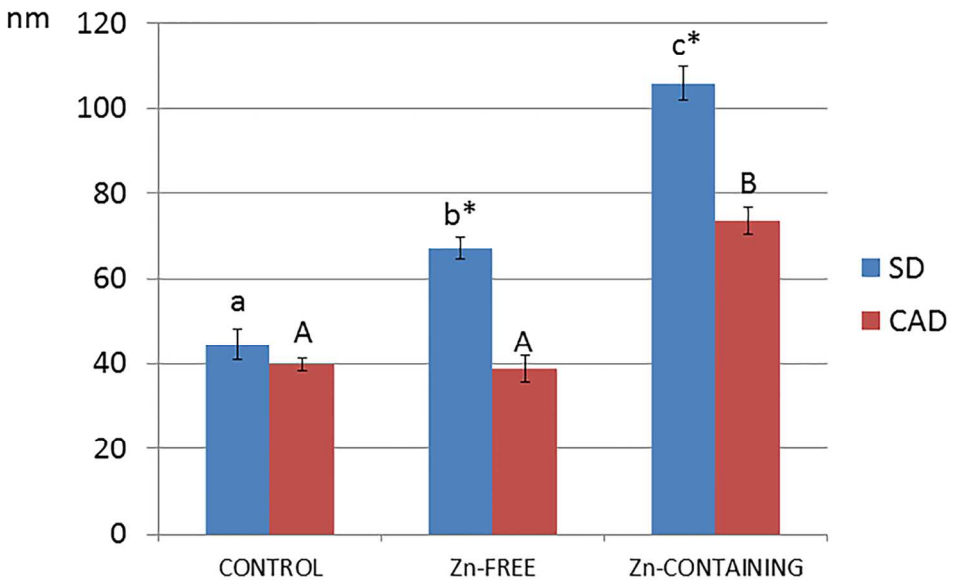

Figure 3. Mean and standard deviation of fibrils width (nm) at sound and caries-affected dentin surfaces, untreated and treated with Zn-free or Zn-containing amalgams. Identical lowercases indicate no significant differences at sound dentin; identical capital letters indicate no significant differences at caries affected dentin.* indicates differences between SD and CAD. Abbreviations: SD: sound dentin, CAD: caries-affected dentin.
121x81mm (300 x 300 DPI)

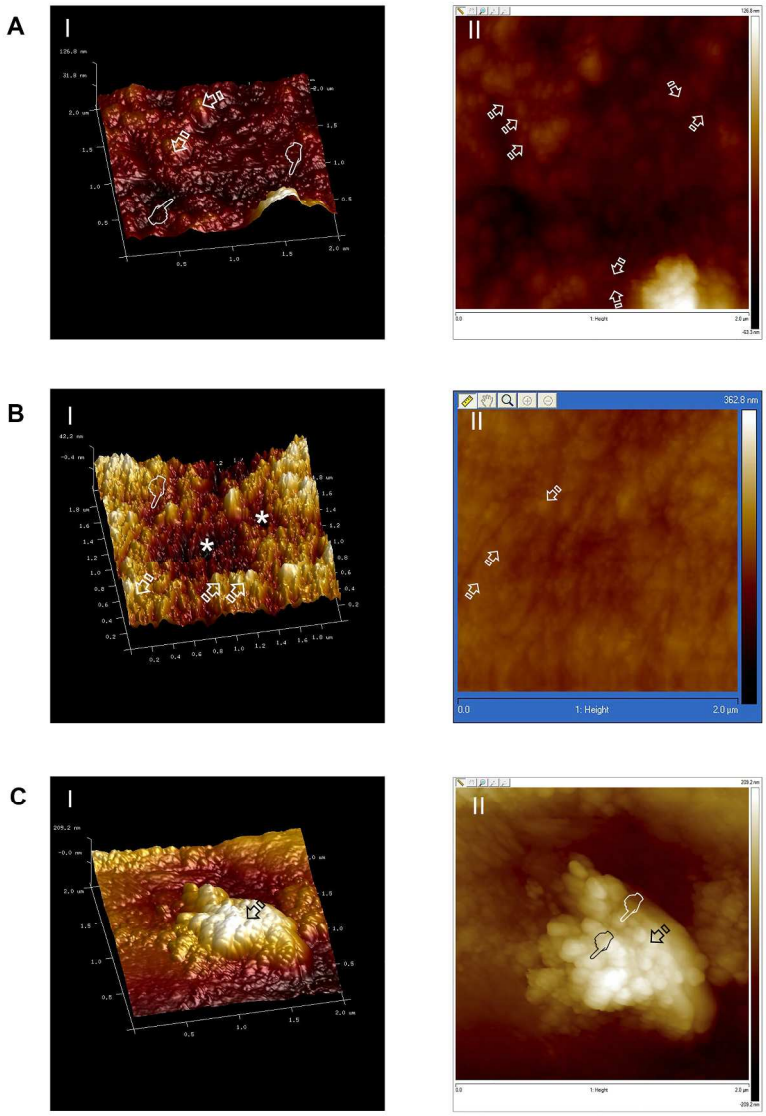

Figure 4. A, AFM images of caries-affected dentin surfaces untreated; AI, 2 x 2 µm top-view and surface plot image of partially demineralized collagen fibrils (arrows), limiting mineral-depleted areas (pointers); AII, AFM phase image (2 x 2 µm) showing the collagen fibrils (arrows). B, AFM images of caries-affected dentin surface restored with Zn-free amalgam. BI, 2 x 2 µm top-view and surface plot image of partially remineralized collagen fibrils (arrows) which show some limited mineral-depleted areas (pointers) as well as the entrance of a some tubules (asterisks); BII, AFM phase image (2 x 2 µm) showing the bandwidth of the collagen fibrils (arrows). C, AFM images of caries-affected dentin surface restored with Zn-containing amalgam; CI, 2 x 2 µm top-view and surface plot image of the advanced remineralized collagen fibrils (arrow); CII, AFM phase image (2 x 2 µm) showing the wider bandwidth of the collagen fibrils (arrows) and the staggered pattern of collagen fibrils (pointers).
261x380mm (300 x 300 DPI)